agronomy

MDPI

*Article*

# UAV-Based Remote Sensing to Evaluate Daily Water Demand Characteristics of Maize: A Case Study from Yuci Lifang Organic Dry Farming Experimental Base in Jinzhong City, China

**Yaoyu Li [1,†], Tengteng Qu [2,†], Yuzhi Wang [2], Qixin Zhao [2], Shujie Jia [2], Zhe Yin [2], Zhaodong Guo [2], Guofang Wang [3], Fuzhong Li [2] and Wuping Zhang [2,*]**

[1] College of Agricultural Engineering, Shanxi Agricultural University, Taigu 030801, China; liyaoyu1998@126.com
[2] College of Software, Shanxi Agricultural University, Taigu 030801, China; work788@163.com (T.Q.); wyzn98@163.com (Y.W.); zhaoqixin6@163.com (Q.Z.); 18834106881@163.com (S.J.); yinz9949@126.com (Z.Y.); g1307256189@126.com (Z.G.); lifuzhong@sxau.edu.cn (F.L.)
[3] College of Resources and Environment, Shanxi Agricultural University, Taigu 030801, China; guofang19800104@126.com
* Correspondence: zwping@126.com
† These authors contributed equally to this work.

**Abstract:** Soil moisture critically influences crop growth, especially in dryland environments. Precise agricultural management requires real-time monitoring of stratified soil moisture and assessment of crops' daily water needs. We aim to provide low-cost, high-throughput information acquisition services for dryland regions with underdeveloped infrastructure and offer scientific support for sustainable water resource management. We used UAVs (Unmanned Aerial Vehicles) with multi-spectral sensors for routine maize monitoring, capturing leaf reflectance. Constructing vegetation indices, we quantified the relationship between leaf water content and surface soil moisture, using the Biswas model to predict deep soil moisture distribution. We used UVAs to monitor crop height and calculated the daily water demand for the entire growth period of corn using the Penman Montes equation. We found an $R^2$ of 0.8603, RMSE of 2.455%, and MAE of 2.099% between NDVI and canopy leaf water content. A strong linear correlation ($R^2$ = 0.7510) between canopy leaf water content and soil moisture was observed in the top 20 cm of soil. Deep soil moisture inversion from the top 20 cm soil moisture showed an $R^2$ of 0.9984, with RE mostly under 10%, but exceeding 20% at 120 cm depth. We also constructed a maize height model aligning with a sigmoidal growth curve ($R^2$ = 0.9724). Maize's daily water demand varied from 0.7121 to 9.4263 mm, exhibiting a downward-opening parabolic trend. Integration of rainfall and soil water data allowed for dynamic irrigation adjustments, mitigating drought and water stress effects on crops. We highlighted UAV multi-spectral imaging's effectiveness in monitoring crop water needs, facilitating quick daily water requirement estimations. Our work offers a scientific foundation for managing maize cultivation in drylands, enhancing water resource utilization.

**Keywords:** UAV; multi-spectral; daily water demand; plant height; soil water storage in layers



**Citation:** Li, Y.; Qu, T.; Wang, Y.; Zhao, Q.; Jia, S.; Yin, Z.; Guo, Z.; Wang, G.; Li, F.; Zhang, W. UAV-Based Remote Sensing to Evaluate Daily Water Demand Characteristics of Maize: A Case Study from Yuci Lifang Organic Dry Farming Experimental Base in Jinzhong City, China. *Agronomy* **2024**, *14*, 729. https://doi.org/10.3390/agronomy14040729

Academic Editor: Mario Cunha

Received: 11 March 2024
Revised: 25 March 2024
Accepted: 29 March 2024
Published: 1 April 2024



## 1. Introduction

Soil moisture is crucial for agricultural production and the hydrological cycle [1,2], especially in arid and semi-arid regions [3]. It is vital for assessing droughts, determining crop yields, and making accurate irrigation decisions [4]. The limitations and spatial discontinuity of traditional soil moisture monitoring methods in large-scale applications have driven the development of remote sensing technology. Specifically, unmanned aerial vehicle (UAV) multi-spectral imaging technology offers unique advantages in providing real-time, extensive coverage of soil moisture and crop biophysical information [5–7]. The

integration of UAV remote sensing technology with machine learning and deep learning has made significant strides in precision agriculture, such as yield estimation, disease identification, and crop classification [8,9]. However, research into real-time monitoring of crop water requirements remains to be further explored. This study explores how remote sensing technology can address conventional methods' limitations in dryland areas with weak infrastructure. It focuses on dynamically monitoring key crop indicators and accurately assessing deep soil moisture content. The goal is to provide a cost-effective, high-throughput service for obtaining crop water demand information, thereby supporting sustainable water resource management.

UAV low-altitude photogrammetry has emerged as an economical supplement to satellite and manned aerial photogrammetry, enhancing the rapid collection and dynamic long-term monitoring of agricultural and forest ecological elements, like vegetation, water bodies, and soil [10]. It has been widely used in dryland areas [7,11,12]. Studying leaf water content is challenging due to its sensitivity to factors like illumination, soil moisture, and air temperature, making accurate and rapid measurement difficult [13,14]. Traditional measurement methods, being time-consuming, labor-intensive, and limited in scope, hinder prompt acquisition of accurate, large-scale monitoring data [15]. Zhen et al. [16] used partial least squares regression and feature band extraction techniques to predict winter wheat leaf water content. Sun and colleagues developed a hyperspectral technology-based quantitative model using PLS-ANN to predict leaf mustard moisture content, achieving an $R^2$ of 0.92 and an RMSE of 2.95% [17,18]. Xu et al. [19] demonstrated a positive correlation between soil moisture and leaf water content. Understanding this interaction is crucial for grasping the dynamics of soil and vegetation in wetlands [20], especially in studies on plant responses to moisture variations [21]. The root system of maize extensively spans the 0–200 cm soil layer, with the majority concentrated in the 0–30 cm range [22]. The mechanisms of root–water interactions highlight the root system's key role in controlling deep soil moisture distribution [23]. Deep water monitoring is vital for precise agriculture, optimizing crop growth, enhancing water efficiency, and improving drought resilience. Although current remote sensing technology effectively gauges surface soil moisture, accurately assessing deep soil moisture demands further research [24]. Current methods to estimate deep soil moisture from surface data involve empirical formulas and machine learning [25,26]. Notably, Biswas et al. [27] created a non-linear model to deduce deep soil moisture from surface data. Yang et al. [28] studied soil moisture variations in winter wheat under various irrigation regimes, finding that irrigation volume and frequency directly influence the accuracy of the Biswas model's parameters. Understanding crop water demand patterns is crucial for developing scientific irrigation strategies. Crop water demand patterns vary with climatic regions, species, and growth stages [29]. In the 1990s, Wang and colleagues conducted the inaugural study on oat water demand in Hebei's Zhangbei [30]. Wang et al. [31] extensively researched oat water demand across 15 urban areas in Northern and Northeastern China. In these studies, scholars [32–34] utilized the FAO-recommended Penman–Monteith formula as their methodology [29,32]. Cheng and colleagues identified a highly significant statistical correlation between spectral-derived and field-measured plant heights [33].

Recent studies highlight the significant potential of remote sensing for monitoring soil moisture [34–36] and assessing crop growth [37]. However, some of these methods face challenges in adaptability across different geographical and climatic conditions, but the limitations are gradually diminishing with advances in small satellite technology and UAV image processing methods [38,39]. Furthermore, current models struggle to accurately reflect crop water demands at specific growth stages. Given these challenges, low-cost, efficient digital monitoring and data acquisition are crucial in dryland areas with limited infrastructure. Utilizing remote sensing technology to collect and analyze soil and crop information not only enhances the productivity of dryland agriculture but also provides crucial information services for underdeveloped regions [40]. The continuous movement of soil moisture between soil, crops, and the atmosphere allows for the estimation and

analysis of moisture processes and footprints using accessible, high-throughput, low-cost data [41].

We conducted an in-depth analysis of spectral data acquired from the DJI Mavic 3 Multi-spectral UAV to calculate vegetation indices and, based on these indices, we developed models correlating with in situ measurements of canopy leaf water content and soil moisture. This approach effectively applies UAV remote sensing technology to the precise monitoring of crop water requirements. The main contributions of our work are as follows. (1) We analyzed the correlation between UAV monitoring data and the dynamics of soil and vegetation moisture. (2) We developed a model for inverting deep soil moisture distribution. (3) We achieved the estimation of daily water requirements throughout the entire growth cycle of crops. (4) Using the full growth cycle of typical maize as the subject of study, we developed an efficient, cost-effective, and user-friendly crop water management model that accurately reflects the water needs of crops at various growth stages. This model can also be extended to other crops or application scenarios, thereby providing scientific decision support for irrigation management.

## 2. Materials and Methods

### *2.1. Overview of the Study Area*

The study was conducted from 9 May to 30 September 2023, at the Yuci Lifang Organic Dry Farming Experimental Base in Jinzhong City, China (37°51′ N, 112°45′ E); the area planted with maize is 80 $m^2$ (10 m × 8 m), as shown in Figure 1. This location is characterized by a warm temperate continental climate, distinct seasonal changes, significant diurnal temperature variations, and prominent arid to semi-arid conditions. Annually, the site receives 2000 to 3000 h of sunshine, has an evaporation rate of 1500 to 2300 mm, a frost-free period of 120 to 220 days, and an elevation ranging from 767 to 1777 m. The annual average temperature is 9.8 °C, with uneven precipitation distribution totaling 418 to 483 mm.

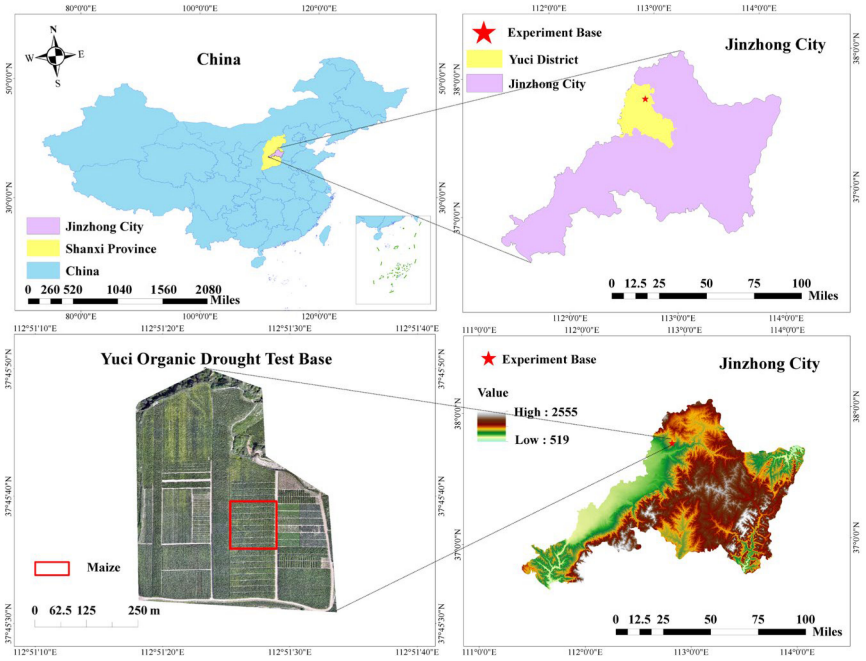


**Figure 1.** Location of the Experiment.

### *2.2. Data Collection and Preprocessing*

#### 2.2.1. Acquisition and Processing of Multi-Spectral Data

The experiment utilized "Chengxin 16" maize, provided by Shanxi Agricultural University, sown on 9 May 2023, emerging on 20 May, and harvested on 6 October. A total of 45 sampling points were established, and 22 high-resolution multi-spectral remote sensing images were collected at a 65 m flying height (Table 1), together with canopy leaf water

content and soil moisture data. The DJI Mavic 3 Multi-spectral UAV system was used, featuring a 4/3-inch visible light CMOS image sensor and a multi-spectral sensor. The acquired multi-spectral images featured four spectral channels: Red (650/16 nm), Green (560/16 nm), Red Edge (730/16 nm), and Near-Infrared (860/26 nm). High-resolution multi-spectral images were captured at 65 m during clear, cloudless weather between 10:00–12:00, ensuring a 70% flight path overlap and 80% side overlap. Two 0.5 m × 1 m control gray boards were used for reflectance correction based on their reflectance. DJI Terra reconstructed the remote sensing images, while ArcMap extracted the spectral reflectance data from the various bands.

**Table 1.** Drone multi-spectral information acquisition.

| Date | Number of Images | Date | Number of Images |
|---|---|---|---|
| 29 June | 5845 | 30 June | 5845 |
| 3 July | 5840 | 5 July | 8260 |
| 7 July | 8265 | 9 July | 8260 |
| 12 July | 8245 | 14 July | 8260 |
| 16 July | 8260 | 18 July | 8260 |
| 21 July | 8265 | 25 July | 8265 |
| 27 July | 8265 | 1 August | 8030 |
| 15 August | 9745 | 24 August | 9515 |
| 20 August | 9740 | 29 August | 9395 |
| 4 September | 9355 | 16 September | 4275 |
| 20 September | 9640 | 30 September | 9700 |

#### 2.2.2. Determination of Canopy Leaf Water Content

Canopy leaf water content data were gathered at the sampling points, with spatial coordinates recorded using a handheld Real-Time Kinematic (RTK). Plant leaves were separated, labeled, and their fresh weight measured. The leaves were placed in an oven at 105 °C for 30 min to deactivate enzymes, then dried at 80 °C until reaching constant weight. The dry weight was then measured to calculate leaf water content using Equation (1) [42].

$$LWC = \frac{FW - DW}{FW} \times 100\% \quad (1)$$

where, *LWC* is the canopy leaf water content; *FW* is the fresh weight of the leaf; and *DW* is the dry weight of the leaf.

#### 2.2.3. Collection and Measurement of Soil Samples

Soil samples were collected at the sampling points using the auger method, and the mass moisture content of the soil layers from 0 to 200 cm was determined by the oven drying and weighing method (Equation (2)) [43]. The bulk density of soil layers from 0 to 200 cm was measured using the core cutter method (Equation (3)) [44]. Three replicates were taken for each layer, with soil moisture indices obtained for the 0–20 cm layer at 10 cm intervals and for the 20–200 cm layers at 20 cm intervals.

$$\theta_m = \frac{m_2 - m_3}{m_3 - m_1} \times 100\% \quad (2)$$

where $\theta_m$ is the soil mass moisture content (g/g); $m_1$ is the weight of the aluminum box (g); $m_2$ is the total weight of the aluminum box and wet soil (g); and $m_3$ is the total weight of the aluminum box and dry soil (g).

$$\rho_s = \frac{m_4 - m_5}{V} \quad (3)$$

The mass moisture content is converted to volumetric moisture content using Equation (4) [45].

$$\theta_V = \frac{\theta_m}{\rho_s} \times 100\% \quad (4)$$

where $\rho_s$ is the bulk density of the soil (g·cm$^{-3}$); $m_4$ is the weight of the core cutter and dry soil (g); $m_5$ is the weight of the core cutter (g); $V$ is the volume of the core cutter (cm$^3$); and $\theta_V$ is the volumetric water content of the soil (%).

2.2.4. Crop Water Requirements

(1) Meteorological Data

Daily meteorological data were downloaded from the National Meteorological Science Data Center, including six key elements: average temperature, maximum temperature, minimum temperature, relative humidity, average wind speed, rainfall, and sunshine duration.

(2) Crop Coefficients

According to the FAO classification standard [29], the maize growth period is classified into an initial stage (36 days), a middle stage (58 days), and a late stage (42 days), with the entire growth cycle extending from 9 May 2023 to 21 September 2023 (136 days).

The FAO recommends $K_{ctable}$ for the initial, mid-, and late stages of maize as 0.51, 1.20, and 0.60, respectively. The crop coefficients for the mid- and late stages are adjusted using Equation (5) [29].

$$K_c = K_{ctable} + [0.04(u_2 - 2) - 0.004(RH_{\min} - 45)][\frac{h}{3}]^{0.3} \quad (5)$$

where $K_{ctable}$ represents the recommended values given by FAO-56, $RH_{\min}$ is the daily average minimum relative humidity (%), $u_2$ is the daily average wind speed at 2 m height (m/s), and $h$ is the average plant height during each growth stage (m).

(3) Reference Crop Water Requirements

The reference crop evapotranspiration is calculated using the FAO-recommended Penman–Monteith equation [29], and the reference crop water requirements are calculated using Equation (6).

$$ET_c = K_c \cdot ET_0 \quad (6)$$

where $ET_c$ is the crop water requirement, in mm/day; $ET_0$ is the reference crop evapotranspiration, in mm/day; and $K_c$ is the crop coefficient.

(4) Crop Height

During the key growth stages of maize, the height of the maize plants was obtained through manual measurements and UAV multi-spectral remote sensing images.

(5) Water Consumption

The water consumption for each growth stage of the growing season is calculated using the water balance equation [46] (Equation (7)).

$$ET = \Delta W + R + I - Q \quad (7)$$

$$\Delta W = S - M \quad (8)$$

where $ET$ is the water consumption, $\Delta W$ is the change in soil moisture within the 0–200 cm soil layer (mm) (Equation (8)), $S$ is the soil moisture content at planting (mm), $M$ is the current soil moisture content (mm), $R$ is the total precipitation during the growing season (mm), $I$ is the irrigation amount (mm; $I = 0$, for this growing season, there was no irrigation), and Q represents surface runoff (mm). Since the experimental site is flat, the Q value is neglected.

### 2.3. Selection of Vegetation Indices

This experiment established 12 primary vegetation indices using the drone's multispectral sensor channels, as detailed in Table 2 [47–50].

**Table 2.** Formulas for Calculating Vegetation Indices.

| Vegetation Indices | Formula |
|---|---|
| Normalized Difference Vegetation Index ($NDVI$) | $NDVI = (NIR - RED)/(NIR + RED)$ |
| Renormalized Difference Vegetation Index ($RDVI$) | $RDVI = (NIR - RED)/\sqrt{NIR + RED}$ |
| Non-linear Vegetation Index ($NLI$) | $NLI = (NIR^2 - RED)/(NIR^2 + GREEN)$ |
| Green Normalized Difference Vegetation Index ($GNDVI$) | $GNDVI = (NIR - GREEN)/(NIR + GREEN)$ |
| Ratio Vegetation Index ($RVI$) | $RVI = NIR/RED$ |
| Soil Adjusted Vegetation Index ($SAVI$) | $SAVI = 1.5(NIR - RED)/(NIR + RED + 0.5)$ |
| Normalized Difference Green Index ($NDGI$) | $NDGI = (GREEN - RED)/(GREEN + RED)$ |
| Wide Dynamic Range Vegetation Index ($WDRVI$) | $WDRVI = (0.2NIR - RED)/(0.2R + RED)$ |
| Optimized Soil Adjusted Vegetation Index ($OSAVI$) | $OSAVI = 1.16(NIR - RED)/(NIR + RED + 0.16)$ |
| Greenness Index ($GI$) | $GI = GREEN/RED$ |
| Modified Simple Ratio ($MSR$) | $MSR = (NIR/RED - 1)/\sqrt{NIR/(RED + 1)}$ |
| Ratio Vegetation Index 2 ($RVI2$) | $RVI2 = NIR/GREEN$ |

### 2.4. Model Construction and Evaluation

We employed UAV spectral remote sensing technology, proceeding from remote sensing data collection, ground data verification, and statistical analysis to model inversion, ultimately to construct a research method for evaluating daily water requirements of maize (Figure 2).

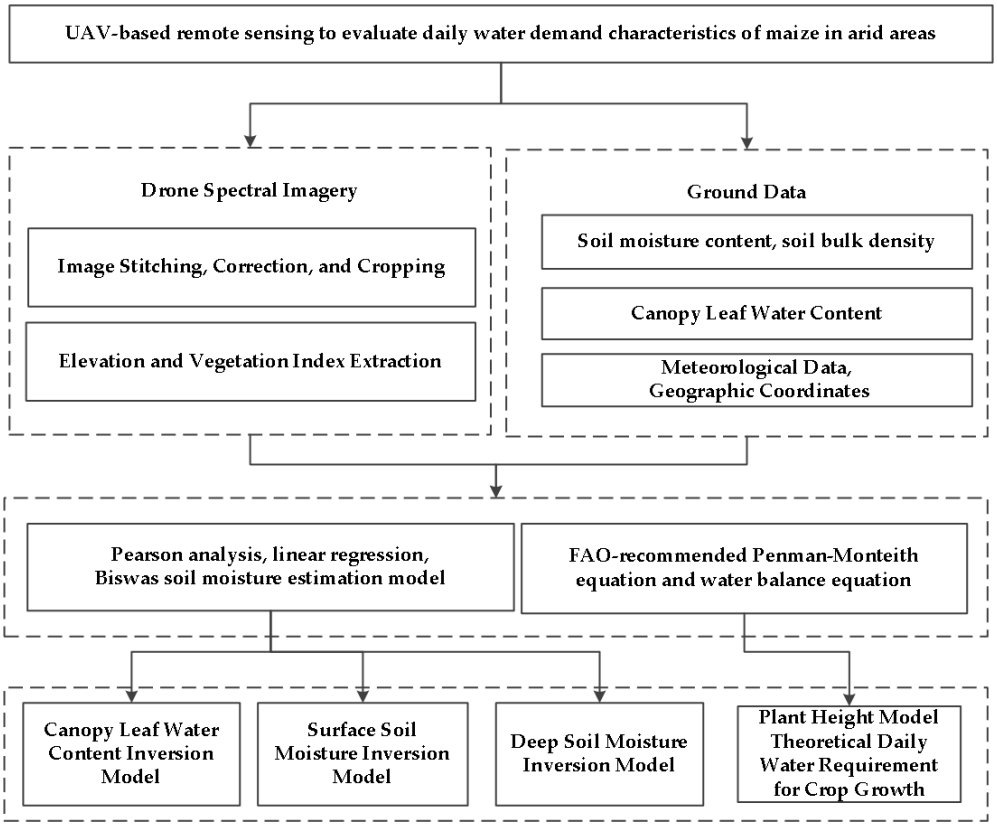


**Figure 2.** Technology Roadmap.

The Biswas soil moisture monitoring model [27] is designed to simulate and forecast soil moisture dynamics. Using actual measurement data, the model's capability to estimate

soil moisture content from 0 to 200 cm depth has been verified and evaluated based on the Biswas soil moisture estimation model.

$$S = A \times (d - d_0) + S_0 \times \left[1 + B \times (d - d_0)^2\right] + S_C \quad (9)$$

where $S$ is the moisture storage within the 0–d cm soil layer, $S_0$ is the moisture storage of the soil's surface layer in cm. $A$, $B$, and $S_C$ are constants that quantify the non-linear relationship between the moisture storage in the surface and deeper soil layers.

To establish the Biswas model, it is essential to initially deduce the three coefficients $A$, $B$, and $S_C$. For the sake of simplifying calculations, Equation (9) is transformed accordingly.

$$S - S_0 = S_C + A \times (d - d_0) + B \times S_0 \times (d - d_0)^2 \quad (10)$$

Set $y = S - S_0$; $x_1 = (d - d_0)$; $x_2 = S_0 \times (d - d_0)^2$; with these substitutions, Formula (9) is transformed accordingly.

$$y = Ax_1 + Bx_2 + S_C \quad (11)$$

We adopted Pearson correlation and regression analysis methods [51], along with the Biswas model [27], to study the relationships between vegetation indices and leaf water content, leaf water content and surface soil moisture, as well as surface soil moisture and deep soil moisture at 0–200 cm. A total of 80% of the maize data was used for modeling and the remaining 20% for validation [52]. The model was evaluated using Root Mean Square Error (RMSE), Mean Absolute Error (MAE), Coefficient of Determination ($R^2$), and Relative Error (RE) as metrics.

## 3. Results

### *3.1. Developing and Validating Models for Vegetation Indices Based on Canopy Leaf Water Content*

We initially assessed the linear relationship between the vegetation indices and the maize canopy leaf water content using scatter plots. Pearson correlation analysis [51] reveals that all 12 vegetation indices [47–50] are highly correlated with maize canopy leaf water content, achieving extremely significant levels ($p < 0.01$) (Table 3). The correlation coefficients (R) range from 0.768 to 0.898, indicating strong positive correlations suitable for quantitatively monitoring vegetation water status through remote sensing.

**Table 3.** Correlation between Vegetation Indices and Canopy Leaf Water Content.

| Vegetation Index | Correlation | Vegetation Index | Correlation | Vegetation Index | Correlation |
|---|---|---|---|---|---|
| WDRVI | 0.898 ** | RVI | 0.898 ** | MSR | 0.898 ** |
| NDGI | 0.891 ** | NDVI | 0.889 ** | SAVI | 0.889 ** |
| RVI2 | 0.882 ** | GI | 0.878 ** | GNDVI | 0.861 ** |
| NLI | 0.842 ** | OSAVI | 0.834 ** | RDVI | 0.768 ** |

Note: ** indicates significance test $p < 0.01$.

To maintain the simplicity of the model, the six vegetation indices with strong correlations (WDRVI, RVI, MSR, NDGI, NDVI, SAVI) were selected to construct linear and non-linear regression models to study the quantitative relationship between maize vegetation indices and canopy leaf water content (Table 4). The non-linear models of the selected six vegetation indices and their linear counterparts exhibited adjusted $R^2$ values ranging from 0.78423 to 0.84910. The quadratic polynomial model of NDVI had the highest adjusted $R^2$, which is 0.84910.

**Table 4.** Univariate Regression Models of Maize Vegetation Indices with Canopy Leaf Water Content.

| Vegetation Index | Model | Formula | Adjusted $R^2$ |
|---|---|---|---|
| NDVI | linear regression | $y = 0.8077\,x + 0.0680$ | 0.78430 |
| | non-linear regression | $y = 3.0852\,x^2 - 3.5396\,x + 1.5667$ | 0.84910 |
| RVI | linear regression | $y = 0.0282\,x + 0.4213$ | 0.80938 |
| | non-linear regression | $y = -0.0009\,x^2 + 0.0427\,x + 0.3677$ | 0.80586 |
| SAVI | linear regression | $y = 0.5386\,x + 0.0679$ | 0.78423 |
| | non-linear regression | $y = 1.3722\,x^2 - 2.3615\,x + 1.5675$ | 0.84907 |
| MSR | linear regression | $y = 0.5386\,x + 0.0679$ | 0.83007 |
| | non-linear regression | $y = 1.3722\,x^2 - 2.3615\,x + 1.5675$ | 0.82761 |
| NDGI | linear regression | $y = 0.9709\,x + 0.4905$ | 0.81456 |
| | non-linear regression | $y = 0.3919\,x^2 + 0.8429\,x + 0.4982$ | 0.80780 |
| WDRVI | linear regression | $y = 0.1695\,x + 0.5625$ | 0.80938 |
| | non-linear regression | $y = -0.0311\,x^2 + 0.2042\,x + 0.5595$ | 0.80586 |

We analyzed the linear models for the RVI, NDGI, WDRVI, and MSR vegetation indices and the non-linear models for the NDVI and SAVI vegetation indices, based on both simulated and observed values (Figure 3). Specifically, NDVI exhibited the lowest RMSE and MAE values, at 2.455% and 2.099%, respectively. Considering various statistical metrics such as adjusted $R^2$, RMSE, and MAE, we selected the NDVI non-linear model to quantify the relationship between vegetation indices and the water content of maize canopy leaves.

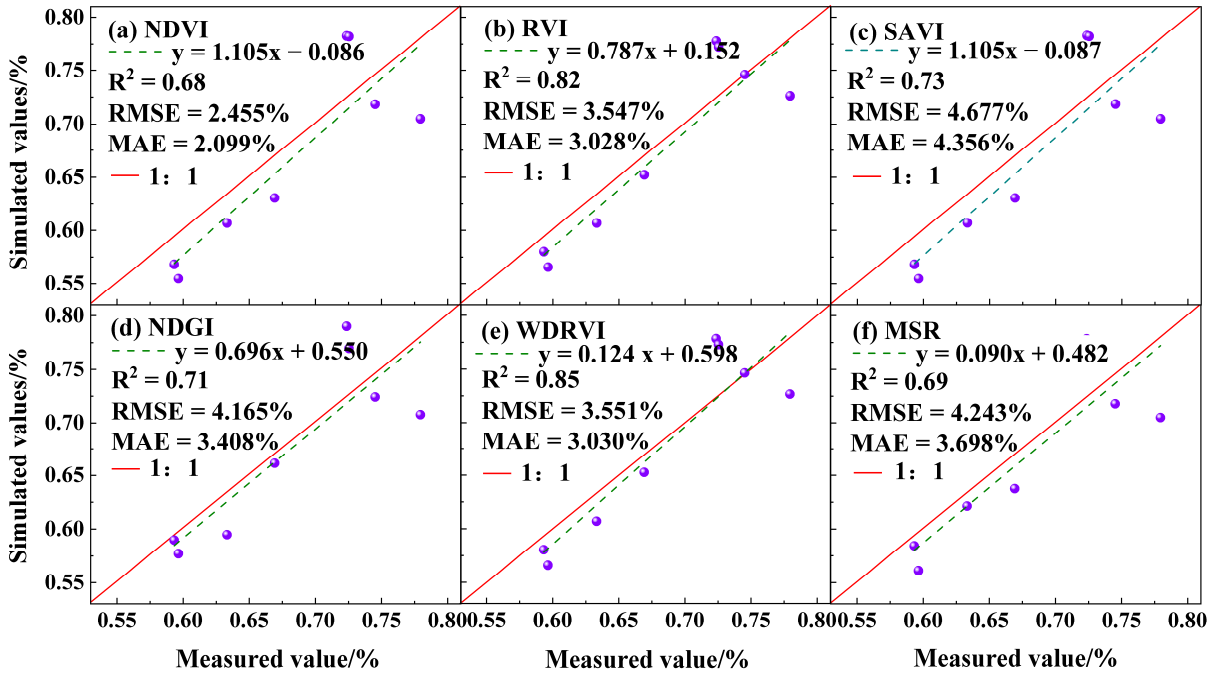


**Figure 3.** Comparison of Simulated and Observed Values of Canopy Leaf Water Content using NDVI (**a**); RVI (**b**); SAVI (**c**); NDGI (**d**); WDRVI (**e**); MSR (**f**).

### *3.2. Model Development and Validation of Canopy Leaf Water Content with Surface Soil Moisture*

We initially assessed the linear relationship between maize canopy leaf water content and surface soil moisture using scatter plots. The Pearson correlation coefficients [51] between the water content of maize canopy leaves and soil moisture at depths of 0–10 cm and 0–20 cm are 0.442 and 0.751, respectively, as shown in Table 5. Within the 0–20 cm soil depth range, the linear relationship between the water content of maize canopy leaves and soil moisture is stronger, as indicated by the model's higher explanatory power.

**Table 5.** Univariate Regression Models of Maize Canopy Leaf Water Content with Different Surface Soil Moisture.

| Depth/cm | Formula | $R^2$ |
|---|---|---|
| 0~10 | y = 0.2953x − 0.0541 | 0.44 |
| 0~20 | y = 0.3831x − 0.0916 | 0.75 |

We analyzed simulated and observed data from linear models correlating maize canopy leaf water content with soil moisture at depths of 0–10 cm and 0–20 cm (Figure 4). The linear model for soil moisture at 0–20 cm depth exhibited the lowest RMSE and MAE, recorded at 2.455% and 2.099%, respectively. Based on various statistical measures, including $R^2$, RMSE, and MAE, we selected the linear model relating maize canopy leaf water content to soil moisture at 0–20 cm depth to quantify the relationship between leaf water content and surface soil moisture.

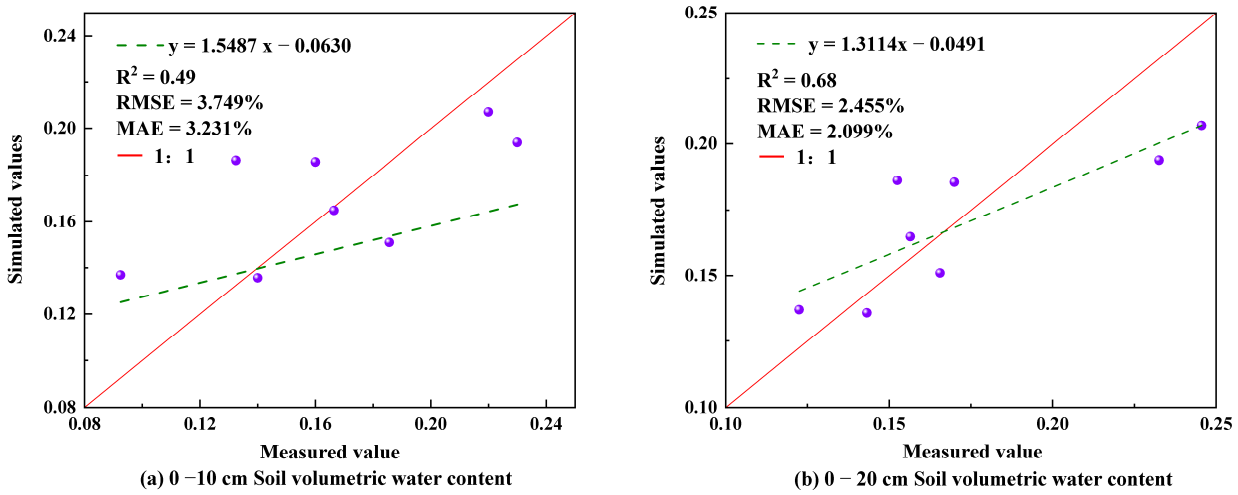


**Figure 4.** Comparison of Predicted and Observed Values of maize Canopy Leaf Water Content with Soil Moisture Content at Depths of 0–10 cm (**a**) and 0–20 cm (**b**).

### *3.3. Biswas Soil Moisture Estimation Model and Validation*

The coefficient of variation quantifies data distribution by measuring the dispersion's absolute value. Typically, a coefficient of variation below 15% signifies a stable data distribution. However, a coefficient of variation above 15% necessitates further situation-specific analysis [53]. The coefficient of variation for soil moisture at varying depths for maize was determined using experimental data, as shown in Table 6. Soil moisture exhibited the highest coefficient of variation in the shallow layer (0–10 cm), with a subsequent decrease in variation as depth increased to 100 cm. Between 120 and 140 cm depth, a minor increase in the coefficient of variation was noted, stabilizing between 12% and 10% beyond 140 cm. These findings suggest a general decrease in the spatial variability of soil moisture for maize with increasing depth. Soil moisture variability is generally lower in the 0–20 cm layer compared to the 0–10 cm layer and remains consistent at deeper layers (>140 cm).

**Table 6.** Variability of Soil Moisture in Different Soil Layers for Maize.

| Soil layer depth/cm | 10 | 20 | 40 | 60 | 80 | 100 | 120 | 140 | 160 | 180 | 200 |
|---|---|---|---|---|---|---|---|---|---|---|---|
| Coefficient of variation/% | 43.97 | 21.22 | 19.44 | 17.52 | 14.06 | 11.23 | 11.05 | 13.29 | 11.25 | 12.43 | 12.03 |

Using the Biswas soil moisture estimation model, we selected two surface soil depths, 0–10 cm and 0–20 cm, as d0 to identify model coefficients for estimating soil moisture in the 0–200 cm profile. We constructed various soil moisture estimation models for maize across different surface layers, as detailed in Table 7. Setting d0 to the 0–20 cm depth range

yielded a high $R^2$ value of 0.9984. This high $R^2$ indicates that the model effectively captures the observed soil moisture variation, demonstrating a strong fit with the measured data.

**Table 7.** Biswas Soil Moisture Estimation Model.

| d0/cm | Biswas Soil Moisture Estimation Model | $R^2$ |
|---|---|---|
| 0–10 | y = 0.108449 x1 − 0.000033 x2 + 0.673764 | 0.9980 |
| 0–20 | y = 0.096848 x1 − 0.000036 x2 + 0.816500 | 0.9984 |

We analyzed simulation and measurement data from the linear model that inverts soil moisture content in the 0–200 cm range, using data from 0–10 cm and 0–20 cm soil layers (Figure 5). For the 0–10 cm depth range inversion, most Relative Error (RE) values are below 10%, suggesting high accuracy in model predictions for this range. However, RE values exceed the 10% threshold at depths like 20 cm, 40 cm, 80 cm, 120 cm, and 200 cm, pointing to reduced model predictive performance at these levels. For the 0–20 cm depth range inversion, relative errors mostly stay below 10%, except for 120 cm, which exceeds 20%. This suggests that data from this range yield more accurate soil moisture predictions. Inversion results for soil moisture in the 0–20 cm depth range are generally more accurate than those for the 0–10 cm range.

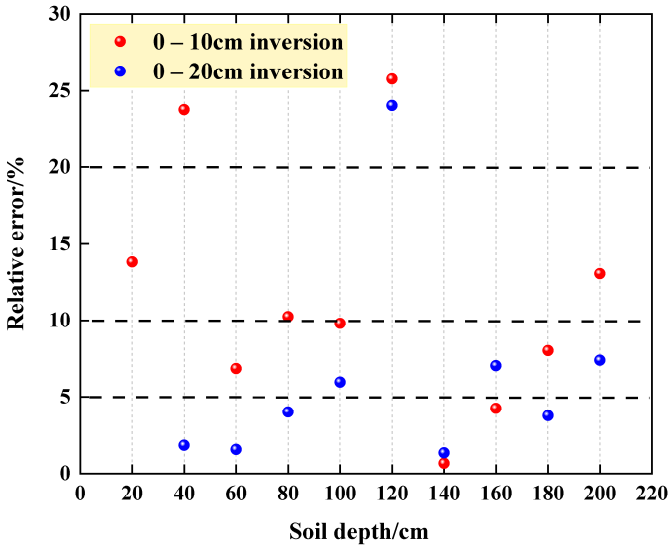


**Figure 5.** Error Distribution of Soil Moisture Content Inversion in Different Soil Layers from 0–200 cm.

### *3.4. Plant Height*

Maize plant height growth followed an "S"-shaped curve, with slow initial growth, an acceleration phase, and a slowdown or plateau in the final stages, as depicted in Figure 6. With an $R^2$ value of 0.9724, the plant height model shows a strong correlation with actual observations, accurately depicting maize height changes over time. Average maize heights during the mid to late growth stages were derived from UAV elevation data, as shown in Table 7.

Based on the experiment and soil water cycle analysis, Shanxi Province's annual rainfall averages around 450 mm, with about five instances of exceptionally heavy rainfall yearly [54]. This pattern does not contribute to groundwater recharge or surface runoff. Additionally, when the groundwater depth exceeds 5 m, it scarcely contributes to the water needs for crop growth.

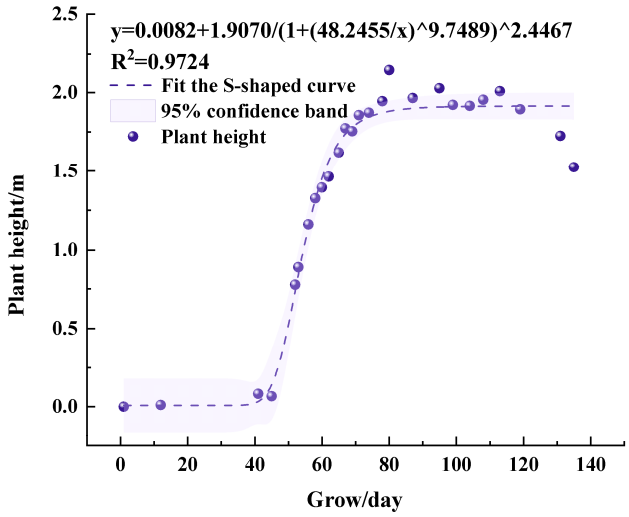


**Figure 6.** Maize plant height from drone elevation monitoring.

During maize's mid- and late growth stages, the minimum average relative humidity was 34.000% and 49.750%, respectively. Meanwhile, the average daily wind speed at 2 m was 2.560 m/s and 1.890 m/s, respectively. The FAO-56 recommended crop coefficients, adjusted for local climatic factors, served as the basis for determining the corrected maize crop coefficients, as shown in Table 8. The corrected crop coefficients directly influence the water requirements of crops, providing an important foundation for our subsequent discussion on crop water needs.

**Table 8.** Average plant height at mid- and late growth stages of maize and crop coefficients.

| Growth Stage | Average Plant Height/m | Crop Coefficient |
|---|---|---|
| Mid-stage | 1.4188 | 1.2531 |
| Late stage | 1.8489 | 0.6342 |

### *3.5. Crop Water Requirements*

This study utilized six meteorological elements and maize growth conditions in the experimental area to calculate the crop's daily water requirements using the P-M formula [29], as illustrated in Figure 7. In the experimental area, the maize's first fertility stage lasted 36 days, followed by a 58-day period of peak water demand, and a later stage of 42 days. During the middle and late fertility stages, the entire experimental area was repeatedly monitored with a drone, from which the vegetation index was derived using spectral data. A non-linear model correlating the vegetation index and NDVI with maize canopy leaf water content was developed. This led to the creation of a linear model linking leaf water content with 0–20 cm soil surface water content. Additionally, soil moisture inversion for 0–20 cm depth facilitated the non-destructive dynamic monitoring of 0–200 cm soil water storage, as depicted in Figure 6.

The theoretical water requirement for maize during its entire reproductive period was 550.368 mm, with 89.267 mm for the early stage, 375.004 mm for the middle stage, and 86.097 mm for the late stage (Figure 8). During the maize's reproductive period, the total rainfall was 208.150 mm, with 33.900 mm in the early stage, 99.100 mm in the middle stage, and 75.150 mm in the late stage. Due to insufficient irrigation, a water deficit of 342.218 mm was observed throughout the reproductive period. The water deficits were 29.616 mm in the early stage, 275.904 mm in the middle stage, and 10.947 mm in the late stage of the reproductive period. During the middle stage of reproduction, the soil's water storage capacity remained largely unchanged after rainfall, suggesting that the rainwater was primarily utilized for crop growth. In the late reproductive stage, the soil's water storage

capacity significantly increased post-rainfall, indicating that the rainwater replenished the soil moisture while supporting crop growth.

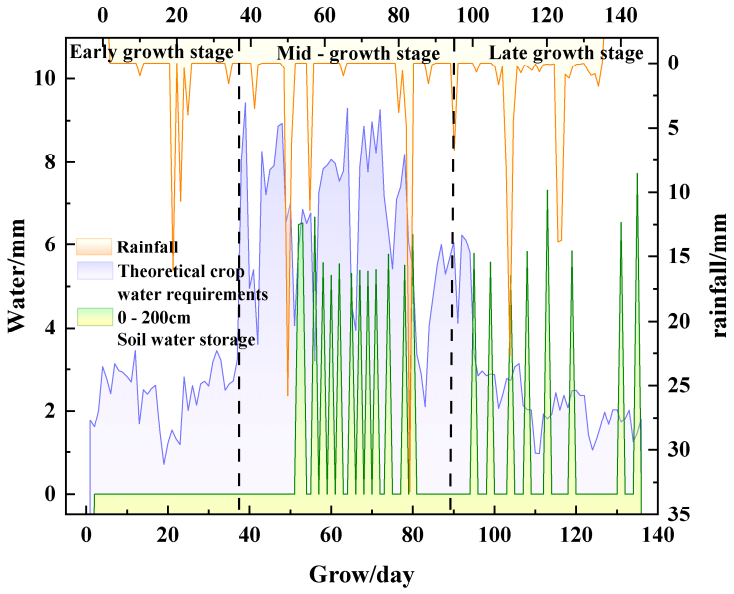


**Figure 7.** Theoretical water requirement, rainfall and soil water storage of maize throughout the reproductive period.

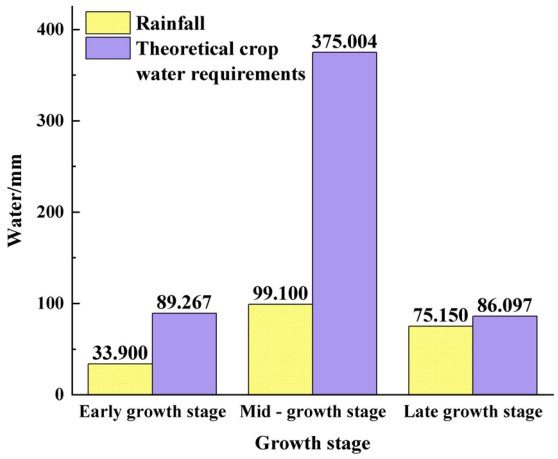


**Figure 8.** Theoretical water requirement and rainfall of maize in each period.

Given the varying water requirements across different growth stages, irrigation strategies must be dynamically tailored to the crop's actual needs to mitigate drought stress impacts on growth. Irrigation management must be optimized according to crop water demands and rainfall patterns to ensure efficient water use and maintain the necessary water balance for crop growth. A scientific approach is required to develop and adjust irrigation schedules, considering factors like crop growth stage, rainfall, and soil water storage. Soil water storage within the 0–200 cm depth is influenced by factors such as rainfall, evapotranspiration, and crop water uptake.

When theoretical water needs exceed rainfall and soil water storage is inadequate, artificial irrigation may be necessary to fulfill the crop's water demands. Excessive rainfall beyond theoretical needs can enhance soil water storage but may lead to drainage or flooding issues due to water surplus. Crop water needs during early, middle, and late maize growth stages vary with the growth phase and biological activities. During early crop fertility, minimal or no irrigation might suffice without hindering seedling emergence. However, in the middle stages, when water demand spikes, irrigation decisions must

be scientifically aligned with soil moisture conditions to maintain crop growth within acceptable stress levels. In the late stages of maize growth, soil reserves generally meet the crop's water requirements, eliminating the need for extra watering.

The study area exhibited a layered soil moisture distribution across the 0–200 cm profile, as shown in Figure 9. We analyzed soil moisture distribution on 3 July and 4 September 2023. Dark blue areas in the figure indicate higher moisture storage in deeper soil layers. The yellow areas denote lower moisture storage in the shallow soil layers. Lower moisture storage in the top soil layer, compared to deeper layers, is attributed to easier evaporation and crop absorption at the surface. Soil moisture distribution shows significant temporal variations. These variations are linked to precipitation, evaporation, and crop uptake. On 4th of September, water storage at both 60 cm and 40 cm depths exceeded levels on 3rd of July. Soil moisture's potential energy depends on depth and water content. Higher moisture in deeper layers implies slower water movement through the soil, necessitating greater root pressure for uptake due to the water's higher potential energy.

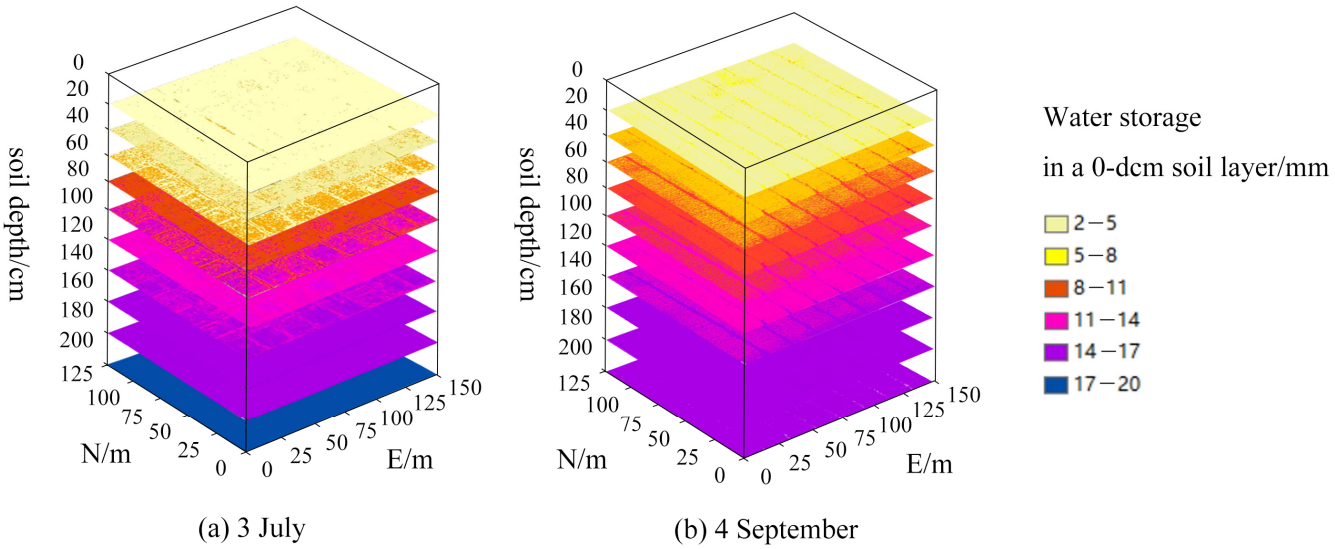


**Figure 9.** Spatial distribution of 0~200 cm soil moisture on 3 July (**a**) and 4 September (**b**), 2023.

Soil moisture storage changes across various soil depths between 29 June and 30 September were derived from spectral data (Figure 10). Maize's actual water consumption was determined to be 190.730 mm. At 20 cm, soil moisture content fluctuations were notably larger and more pronounced. Soil moisture content at 20 cm exhibited obvious fluctuations with a larger amplitude, indicating a higher sensitivity in shallower soil layers to changes influenced by factors such as rainfall, evaporation, and plant water absorption. Fluctuations in soil moisture content above 160 cm were gentler with smaller amplitudes, This suggests relative stability in soil moisture content at these depths, with minimal impact from short-term environmental changes. This reflects how environmental changes differentially affect soil moisture at various depths: shallow soils are more susceptible to daily meteorological variations, whereas deeper soils are influenced more by long-term factors, like groundwater.

Given the variability in water requirements across different growth stages, irrigation strategies must be dynamically tailored to the crops' actual needs to mitigate drought stress. Optimal irrigation management, based on crop water demand and rainfall patterns, ensures efficient water resource use and maintains the necessary water balance for crop growth. Developing and adjusting irrigation schedules scientifically, considering factors like crop growth stage, rainfall, and soil water storage, is essential.

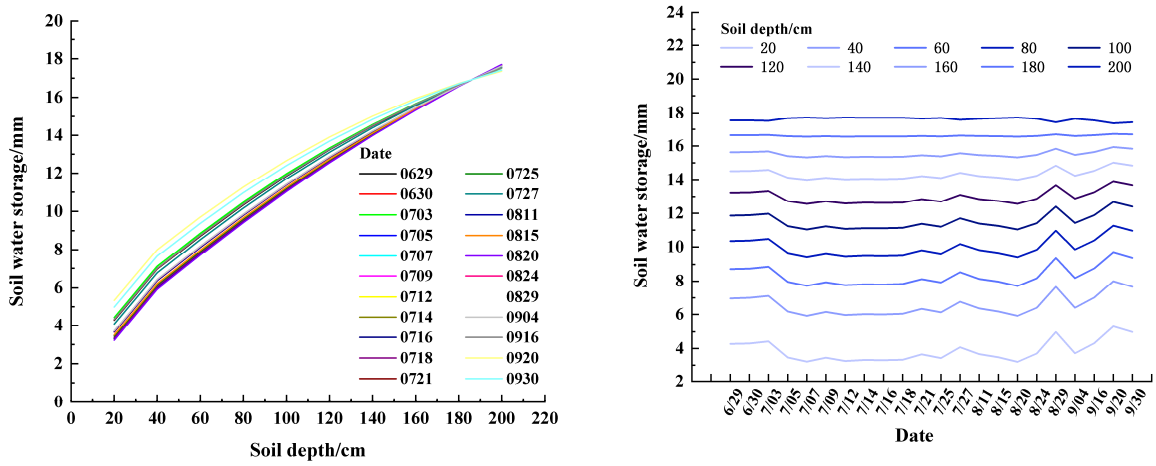


(**a**) (**b**)

**Figure 10.** Moisture storage in the 0~d cm soil layer of maize at 22 days. Display by Soil Depth (**a**); Display by Date (**b**).

## 4. Discussion

UAV multi-spectral remote sensing is increasingly used for extensive soil moisture monitoring in arid regions with crops, marking a significant trend in precision agriculture's evolution [55–57]. This study employed a UAV-mounted spectral sensor to calculate the vegetation index and correlate it with leaf and soil moisture levels. This facilitated dynamic monitoring of crop height and soil moisture distribution, aiding in understanding crop water requirements. The findings offer valuable insights for devising scientific irrigation approaches and enhancing water management in agriculture.

### *4.1. Study of Vegetation Indices, Canopy Leaf Water Content, and Biswas Soil Moisture Estimation Models*

Recently, utilizing various vegetation indices has emerged as a primary method for detecting crop irrigation practices through multi-spectral remote sensing data [58]. This study selected 12 vegetation indices to analyze their correlation with maize leaf water content using UAV spectral data. WDRVI, RVI, MSR, NDGI, NDVI, and SAVI emerged as the most suitable indices for estimating maize leaf water content. Linear and non-linear models were developed to correlate with leaf water content. The performance of the non-linear NDVI model was determined to be superior based on RMSE and MAE metrics [59]. The study found that highly correlated vegetation indices predominantly combined the red, red-edge, and NIR bands. This aligns with the findings of Li et al. The study revealed a significant positive correlation between crop canopy water content and soil surface moisture, aligning with the findings of Aslan et al. [20]. The study refined the selection of soil depth to 0–20 cm, where a stronger correlation (R = 0.751) was observed, enhancing the accuracy of shallow soil moisture estimation. Regarding the Biswas soil moisture estimation model, we selected coefficients apt for the 0–200 cm soil moisture range, demonstrating exceptional explanatory power within the 0–20 cm depth ($R^2$ = 0.9984).This corroborates the findings of Yang et al. [28], which also highlighted the importance of selecting appropriate soil depths in models to enhance performance.

### *4.2. Study on Crop Water Requirements at Different Growth Stages*

This study precisely determined maize's water needs across various growth stages using UAV monitoring and modeling, highlighting the strong link between soil moisture dynamics and maize development. Maize growth followed an "S"-shaped curve, with initial slow growth, faster mid-stage growth, and slower late stage growth, consistent with Ye's observations [60]. Furthermore, the high coefficient of determination ($R^2$ = 0.9724) underscored the model's accuracy in predicting actual plant growth, highlighting its

agricultural importance. This aligns with the findings of He et al. [61], further validating UAV monitoring data's reliability and value in precision agriculture. Differences in soil crop coefficients were marginal, with no significant variance in actual water requirements for the crop. Hence, FAO-56's crop coefficients are deemed fully suitable for arid and semi-arid regions. Soil water transport, a complex process, occurs over various temporal and spatial scales and is influenced by soil's physical, chemical, and microbiological properties [62]. The crop coefficient, which integrates crop type, biological traits, soil moisture, fertilizer condition, and field management, is essential for calculating water requirements [63]. For maize in its mid- to late stages, corrected crop coefficients exceeded FAO's recommendations, likely due to increased water needs in arid areas with high soil evaporation. In the 1990s, Bai determined that maize in Yunnan required 369.7–417.9 mm of water, based on field trials [64]. In the 1970s, Wendt assessed sweet maize's water needs under various irrigation methods in Texas, finding that requirements ranged from 310 to 361 mm during full reproductive stage, determined by monitoring soil water potential [65]. This study found maize's water requirement during the entire reproductive period to be 550.368 mm, higher than previous studies. This discrepancy might stem from significant evaporation between maize plants in arid regions, with Wang indicating evaporation can account for 43.57% to 52.52% of total water loss [66]. Furthermore, factors like weather, soil type, planting density, and farming practices also influence water needs. Sweet maize's water requirement is influenced by multiple factors including weather, soil type, planting density, and cultivation methods. Changes in any of these factors can directly impact water needs. Despite the high water demand observed for maize, the pattern of water usage depicted a downward-opening parabola, aligning with findings by Xiao [67] and Fan [68]. observed that water level fluctuations decreased with soil depth, a finding corroborated by this study. During maize's mid-growth stage, soil water levels remained stable after rainfall, suggesting that the precipitation was utilized for crop growth. At maize's late growth stage, soil water storage increased significantly post-rainfall, indicating that the rainwater contributed to soil moisture in addition to supporting crop growth. Soil water storage at 0–40 cm depth was higher during the mid-growth stage than the late stage, while at 0–200 cm depths, it was lower in the late stage, likely because maize roots efficiently absorb water from 60–100 cm depths. As maize grows, its roots absorb water from shallow depths, drawing deeper water upwards via capillary action, which reduces water at greater depths while increasing it in shallower ones. Monitoring soil moisture up to 200 cm deep allows researchers and farmers to grasp soil water dynamics better, enabling more effective management of water resources to support crop growth and ecological balance.

In conclusion, this study provides a scientific basis for future crop water status monitoring using remote sensing technologies. We compared soil, climate, and planting practices across various arid regions and assessed the applicability of our research methods, finding that, with adjustments, our remote sensing techniques and methods are broadly applicable to most arid areas. We also proposed measures to enhance generalizability, such as developing flexible models and conducting field validations. Moreover, this method has its limitations; the cost can be significant when using UAV data to collect crop information across an entire city. Future research should explore the direct involvement of spectral bands in model establishment, and universality under different crop planting densities, climatic, and soil conditions, to achieve long-term, high-precision monitoring of soil moisture in agricultural areas. This will provide a theoretical basis for quantitative evaluation of arable crops in arid regions and the determination of irrigation systems, ultimately offering technical guidance for the management of arid lands, ecological agricultural construction, and development.

## 5. Conclusions

This study employed UAV multi-spectral technology, integrating vegetation indices with canopy leaf water content and soil moisture data, to quickly estimate soil water

content from 0 to 200 cm under dry farming conditions, enabling daily assessment of crop water needs.

All 12 maize vegetation indices showed a strong correlation with leaf water content at the 0.01 significance level. Among the top 6 indices, the NDVI non-linear model was the most accurate.

Maize canopy leaf water content proved to be an effective indicator for estimating surface soil moisture, particularly with high model accuracy at soil depths of 0 to 20 cm.

The variability in soil water content decreased with depth, suggesting that soil moisture variation diminishes as depth increases. Soil moisture variability at 0 to 20 cm was generally lower than at 0 to 10 cm and stabilized in deeper layers beyond 140 cm. Applying the Biswas model to various soil surface water contents at 0 to 200 cm depths showed that the 20 cm model exhibited higher $R^2$ and RE values than the 10 cm model, indicating its greater accuracy and effectiveness in enhancing deep soil moisture estimation accuracy.

The model enabled non-destructive, dynamic UAV monitoring of soil water storage from 0 to 200 cm. During maize's mid-growth stage, water storage remained stable, but it increased in the late reproductive stage with more rainfall.

UAVs facilitated dynamic monitoring of maize height, confirming its adherence to an "S"-shaped growth curve. By calculating average heights and adjusting crop coefficients with meteorological data, we found mid- and late stage coefficients to be 1.2531 and 0.6342, respectively. The maize's daily water demand, depicted by a downward-opening parabola, was also calculated. Integrating soil water storage data, we identified varying degrees of water deficit across all maize growth stages, in order to develop a scientific field water management strategy.

**Author Contributions:** Conceptualization, Y.L., T.Q. and Y.W.; methodology, Y.L., T.Q. and Y.W.; software, Y.L., T.Q. and Q.Z.; validation, Y.L. and S.J.; formal analysis, Y.L. and Z.G.; data curation, Y.L., S.J. and Z.Y.; writing—original draft preparation, Y.L. and T.Q.; writing—review and editing, Y.L. and W.Z.; visualization, Y.L. and G.W.; supervision F.L.; project administration F.L.; funding acquisition, F.L. and W.Z. All authors have read and agreed to the published version of the manuscript.

**Funding:** The research and the APC was funded by The National Key Research and Development Program Project (No. 2021YFD1901101-5); Key Research and Development Project in Shanxi Province (No. 202202140601021); and the Basic Research Project of Shanxi Provincial Department of Science and Technology (No. 202103021224123).

**Data Availability Statement:** The original contributions presented in the study are included in the article, further inquiries can be directed to the corresponding author.

**Conflicts of Interest:** The authors declare no conflicts of interest.

## References

1. Timbal, B.; Power, S.; Colman, R.; Viviand, J.; Lirola, S. Does Soil Moisture Influence Climate Variability and Predictability over Australia? *J. Clim.* **2002**, *15*, 1230–1238. [CrossRef]
2. Jingling, C.; Peishu, W.; Linqi, L.; Qian, W.; Xu, W.; Xitian, Y.; Jinsong, Z.; University, H.A. Impacts of radiation, temperature and soil moisture on hidden heat of transpiration and leaf temperature of *Quercus variabilis* seedlings. *Sci. Soil Water Conserv.* **2017**, *15*, 62.
3. Wang, A.; Ma, X. An overview of soil moisture drought research in China:Progress and perspective. *Atmos. Ocean. Sci. Lett.* **2023**, *16*, 22–27.
4. Dorigo, W.; Himmelbauer, I.; Aberer, D.; Sabia, R. The International Soil Moisture Network: Serving Earth system science for over a decade. *Hydrol. Earth Syst. Sci.* **2021**, *25*, 5749–5804. [CrossRef]
5. Junying, C.; Xintao, W.; Zhitao, Z.; Jia, H.; Zhihua, Y.; Guangfei, W. Soil Salinization Monitoring Method Based on UAV-Satellite Remote Sensing Scale-up. *Trans. Chin. Soc. Agric. Mach.* **2019**, *50*, 161–169.
6. Xianfeng, Z. Co-Inversion and Validation of Large-Area Soil Moisture Based on Modis and Amsr-E Data. *Acta Pedol. Sin.* **2012**, *49*, 205–211.
7. Singh, A.; Kumar, S.; Duhan, D.; Kumar, N.; Dhaloiya, A.; Kumar, M. Assessment of Soil Water Dynamics and Yield Response of Broccoli Under Subsurface Drip Irrigation in the Semi-Arid Region of India. *Commun. Soil Sci. Plant Anal.* **2023**, *55*, 636–652. [CrossRef]
8. Shahi, T.B.; Xu, C.-Y.; Neupane, A.; Guo, W. Recent Advances in Crop Disease Detection Using UAV and Deep Learning Techniques. *Remote Sens.* **2023**, *15*, 2450. [CrossRef]

9. Shahi, T.B.; Xu, C.-Y.; Neupane, A.; Guo, W. Machine learning methods for precision agriculture with UAV imagery: A review. *Electron. Res. Arch.* **2022**, *30*, 4277–4317. [CrossRef]
10. Ilniyaz, O.; Du, Q.; Shen, H.; He, W.; Feng, L.; Azadi, H.; Kurban, A.; Chen, X. Leaf area index estimation of pergola-trained vineyards in arid regions using classical and deep learning methods based on UAV-based RGB images. *Comput. Electron. Agric.* **2023**, *14*, 415. [CrossRef]
11. Rongqiang, G.; Shifu, F. Principles and applications of modern near infrared spectroscopic techniques. *Anal. Instrum.* **2002**, *3*, 9–12.
12. Sergent, A.S.; Segura, V.; Charpentier, J.P.; Dalla-Salda, G.; Martinez-Meier, A. Assessment of resistance to xylem cavitation in cordilleran cypress using near-infrared spectroscopy. *For. Ecol. Manag.* **2020**, *462*, 117943. [CrossRef]
13. Sun, C.B.; Fan, X.W.; Hu, H.Y.; Liang, Y.; Li, Y.Z. Pivotal metabolic pathways related to water deficit tolerance and growth recovery of whole maize plant. *Plant Omics* **2013**, *6*, 377–387.
14. Zheng, X.J.; Song, L.I.; Yan, L.I. Leaf water uptake strategy of desert plants in the Junggar Basin, China. *Chin. J. Plant Ecol.* **2011**, *35*, 893–905. [CrossRef]
15. Xie, C.; Shao, Y.; Li, X.; He, Y. Detection of early blight and late blight diseases on tomato leaves using hyperspectral imaging. *Sci. Rep.* **2015**, *5*, 16564. [CrossRef] [PubMed]
16. Martinelli, F.; Scalenghe, R.; Davino, S.; Panno, S.; Scuderi, G.; Ruisi, P.; Villa, P.; Stroppiana, D.; Boschetti, M.; Goulart, L.R. Advanced methods of plant disease detection. A review. *Agron. Sustain. Dev.* **2015**, *35*, 1–25. [CrossRef]
17. Sun, J.; Cong, S.; Mao, H.; Wu, X.; Zhang, X.; Wang, P. CARS-ABC-SVR model for predicting leaf moisture of leaf-used lettuce based on hyperspectral. *Trans. Chin. Soc. Agric. Eng.* **2017**, *33*, 178–184.
18. Jun, S.; Xiao-Hong, W.U.; Xiao-Dong, Z. Research on Lettuce Leaves' Moisture Prediction Based on Hyperspectral Images. *Spectrosc. Spectr. Anal.* **2013**, *33*, 522–526.
19. Zheng, S.; Lan, Z.; Li, W.; Shao, R.; Shan, Y.; Wan, H.; Taube, F.; Bai, Y. Differential responses of plant functional trait to grazing between two contrasting dominant C3 and C4 species in a typical steppe of Inner Mongolia, China. *Plant Soil* **2011**, *340*, 141–155. [CrossRef]
20. Aslan, F.; Prado-Tarango, D.E.; Mata-González, R.; Godwin, D.; Ochoa, C.G. Soil Water Content and Its Interaction with Plant Water Potential in a Conservation Wetland. In Proceedings of the Society for Range Management Annual Meeting, Denver, CO, USA, 16–20 February 2020.
21. Amatya, S.; Karkee, M.; Alva, A.K. Identifying Water Stress in Potatoes Using Leaf Reflectance as an Indicator of Soil Water Content. *GSTF J. Agric. Eng.* **2014**, *1*, 52–61. [CrossRef]
22. Jiang, Z.; Zhang, Y.-m.; Xing-kui, N. Studies on the distribution of maize root characteristics at different soil layers and densities. *Acta Agric. BorealiGSinica* **2011**, *26*, 99–103.
23. Maan, C.; ten Veldhuis, M.C.; van de Wiel, B.J.H. Dynamic root growth in response to depth-varying soil moisture availability: A rhizobox study. *Hydrol. Earth Syst. Sci.* **2023**, *27*, 2341–2355. [CrossRef]
24. Tan, C.; Zhang, Z.; Xu, C.; Ma, Y.; Yao, Z.; Wei, G.; Li, Y. Soil water content inversion model in field maize root zone based on UAV multispectral remote sensing. *Trans. Chin. Soc. Agric. Eng.* **2020**, *36*, 63–74.
25. Yueh, S.H.; Shah, R.; Chaubell, M.J.; Hayashi, A.; Colliander, A. A Semiempirical Modeling of Soil Moisture, Vegetation, and Surface Roughness Impact on CYGNSS Reflectometry Data. *IEEE Trans. Geosci. Remote Sens.* **2020**, *60*, 5800117. [CrossRef]
26. Senyurek, V.; Lei, F.; Boyd, D.; Kurum, M.; Moorhead, R. Machine Learning-Based CYGNSS Soil Moisture Estimates over ISMN sites in CONUS. *Remote Sens.* **2020**, *12*, 1168. [CrossRef]
27. Biswas, B.C.; Dasgupta, S.K. Estimation of soil moisture at deeper depth from surface layer data. *Mausam* **1979**, *30*, 511–516. [CrossRef]
28. Yang, J.; Cai, H.; Wang, S.; Xie, H. Relationship between soil moisture in surface layer and in deeper depth in Yangling. *Agric. Res. Arid. Areas* **2010**, *28*, 53–57.
29. Allen, R.G.; Pereira, L.S.; Raes, D.; Smith, M. *Crop Evapotranspiration—Guidelines for Computing Crop Water Requirements*; FAO Irrigation and Drainage Paper 56; FAO: Rome, Italy, 1998; Volume 300, p. D05109.
30. Wu, W.D.; Da, W.H.; Qing, L.S.; Zhi, X.J.; Tai, G.R. Soil Properties and Precipitation Potential Productivity Response to Fertilizer Application in Cold Highland semiarid Region. *Acta Tritical Crops* **2000**, *2*, 60–65.
31. Wang, C.; Lin, Q.; Shi, X.-Y.; Li, S.; Jie, X.-J.; Chu, Q.-Q. Assessment on water requirement of oat in different areas using SIMETAW model. *J. Agric. Sci. Technol.* **2020**, *22*, 131–139.
32. Doorenbos, J.; Pruitt, W.O. *Guidelines for Predicting Crop Water Requirements*; Food and Agriculture Organization of the United Nations: Washington, DC, USA, 1977.
33. Chen, Z.; Cheng, Q.-A.; Xu, H.-G.; Huang, X.-Q. Inversion Model of Summer Maize Plant Height and Biomass under Different Water and Fertilizer Treatments Based on UAV Spectra. *Agric. Res. Arid. Areas* **2023**, *4*, 198–207.
34. Prodhan, F.A.; Zhang, J.; Yao, F.; Shi, L.; Pangali Sharma, T.P.; Zhang, D.; Cao, D.; Zheng, M.; Ahmed, N.; Mohana, H.P. Deep learning for monitoring agricultural drought in South Asia using remote sensing data. *Remote Sens.* **2021**, *13*, 1715. [CrossRef]
35. Zhang, A.; Jia, G. Monitoring meteorological drought in semiarid regions using multi-sensor microwave remote sensing data. *Remote Sens. Environ.* **2013**, *134*, 12–23. [CrossRef]
36. Bhavani, P.; Roy, P.; Chakravarthi, V.; Kanawade, V.P. Satellite remote sensing for monitoring agriculture growth and agricultural drought vulnerability using long-term (1982–2015) climate variability and socio-economic data set. *Proc. Natl. Acad. Sci. India Sect. A Phys. Sci.* **2017**, *87*, 733–750. [CrossRef]
37. Kasampalis, D.A.; Alexandridis, T.K.; Deva, C.; Challinor, A.; Moshou, D.; Zalidis, G. Contribution of remote sensing on crop models: A review. *J. Imaging* **2018**, *4*, 52. [CrossRef]

38. Li, M.; Sun, H.; Zhao, R. A Review of Root Zone Soil Moisture Estimation Methods Based on Remote Sensing. *Remote Sens.* **2023**, *15*, 5361. [CrossRef]
39. Alijani, Z.; Eyre, R.; Saurette, D.; Laamrani, A.; Lindsay, J.; Western, A.; Berg, A. An efficient soil moisture sampling scheme for the improvement of remotely sensed soil moisture validation over an agricultural field. *Geoderma* **2024**, *442*, 116763. [CrossRef]
40. Paolini, G.; Escorihuela, M.J.; Bellvert, J.; Merlin, O.; Pellarin, T. PrISM at Operational Scale: Monitoring Irrigation District Water Use during Droughts. *Remote Sens.* **2024**, *16*, 1116. [CrossRef]
41. Chang, X.; Chang, G. Advances in research and prospect on soil moisture in arid and semi-arid areas. *J. Desert Res.* **2021**, *41*, 156.
42. Reynolds, S. The gravimetric method of soil moisture determination Part IA study of equipment, and methodological problems. *J. Hydrol.* **1970**, *11*, 258–273. [CrossRef]
43. Zhang, Q.; Min, L.; Wang, Y.; Zhu, Y.; Jia, M.; Sun, K.; Shen, Y. Accuracies of soil moisture sensors in typical soils in the Hebei Plain. *Chin. J. Eco-Agric.* **2023**, *31*, 1851–1859.
44. Eltarabily, M.G.; Mohamed, A.Z.; Begna, S.; Wang, D.; Putnam, D.H.; Scudiero, E.; Bali, K.M. Simulated soil water distribution patterns and water use of Alfalfa under different subsurface drip irrigation depths. *Agric. Water Manag.* **2024**, *293*, 108693. [CrossRef]
45. Sun, T.; Li, Z.; Wu, Q.; Sheng, T.; Du, M. Effects of alfalfa intercropping on crop yield, water use efficiency, and overall economic benefit in the Corn Belt of Northeast China. *Field Crops Res.* **2018**, *216*, 109–119. [CrossRef]
46. Adler, J.; Parmryd, I. Quantifying colocalization by correlation: The Pearson correlation coefficient is superior to the Mander's overlap coefficient. *Cytom. Part A* **2010**, *77*, 733–742. [CrossRef] [PubMed]
47. Mishra, S.; Mishra, D.R. Normalized difference chlorophyll index: A novel model for remote estimation of chlorophyll-a concentration in turbid productive waters. *Remote Sens. Environ.* **2012**, *117*, 394–406. [CrossRef]
48. Rouse, J.W., Jr.; Haas, R.H.; Deering, D.; Schell, J.; Harlan, J.C. Monitoring the Vernal Advancement and Retrogradation (Green Wave Effect) of Natural Vegetation; Earth Resources and Remote Sensing, United States. 1974. Available online: https://ntrs.nasa.gov/citations/19750020419 (accessed on 10 March 2024).
49. Rondeaux, G.; Steven, M.; Baret, F. Optimization of soil-adjusted vegetation indices. *Remote Sens. Environ.* **1996**, *55*, 95–107. [CrossRef]
50. Ranjan, R.; Chopra, U.K.; Sahoo, R.N.; Singh, A.K.; Pradhan, S. Assessment of plant nitrogen stress in wheat (*Triticum aestivum* L.) through hyperspectral indices. *Int. J. Remote Sens.* **2012**, *33*, 6342–6360. [CrossRef]
51. Cho, D.S.; Chung, C.W.; Kim, J.; Ahn, S.; Park, H.S. Analysis on Reports of Statistical Testings for Correlation and Regression. *Korean J. Women Health Nurs.* **2008**, *14*, 213. [CrossRef]
52. Yinglan, A.; Jiang, X.; Wang, Y.; Wang, L.; Zhang, Z.; Duan, L.; Fang, Q. Study on spatio-temporal simulation and prediction of regional deep soil moisture using machine learning. *J. Contam. Hydrol.* **2023**, *258*, 104235.
53. Zhang, L.; Niu, Y.; Zhang, H.; Han, W.; Tang, J. Maize canopy temperature extracted from UAV thermal and RGB imagery and its application in water stress monitoring. *Front. Plant Sci.* **2019**, *10*, 461668. [CrossRef]
54. Sah, S.S.; Maulud, K.N.A.; Sharil, S.; Karim, O.A.; Pradhan, B. Monitoring of three stages of paddy growth using multispectral vegetation index derived from UAV images. *Egypt. J. Remote Sens. Space Sci.* **2023**, *26*, 989–998.
55. Cheng, M.; Sun, C.; Nie, C.; Liu, S.; Yu, X.; Bai, Y.; Liu, Y.; Meng, L.; Jia, X.; Liu, Y. Evaluation of UAV-based drought indices for crop water conditions monitoring: A case study of summer maize. *Agric. Water Manag.* **2023**, *287*, 108442. [CrossRef]
56. Ma, B.; Hou, Z.; Jiang, Y. Application of UAV Remote Sensing in Monitoring Water Use Efficiency and Biomass of Cotton Plants Adjacent to Shelterbelt. *Front. Plant Sci.* **2022**, *13*, 894172. [CrossRef]
57. Zhang, N.; Su, X.; Zhang, X.; Yao, X.; Cheng, T.; Zhu, Y.; Cao, W.; Tian, Y. Monitoring daily variation of leaf layer photosynthesis in rice using UAV-based multi-spectral imagery and a light response curve model. *Agric. For. Meteorol.* **2020**, *291*, 108098. [CrossRef]
58. Liang, D.; Yang, Q.; Huang, W.; Peng, D.; Song, X. Estimation of leaf area index based on wavelet transform and support vector machine regression in winter wheat. *Infrared Laser Eng.* **2015**, *44*, 335–340.
59. Ye, R. *Study on the Growth and Development Patterns of Corn Plants*; Shanxi Agricultural University: Shanxi, China, 2019.
60. Ying, H.; Nan, Y.; Jinzhi, Y.; Jihua, L. Application of UAV remote sensing technology in maize height extraction. *Surv. Mapp. Technol. Equip.* **2023**, *25*, 83–88.
61. Wang, Z.; Zhang, H.; Yin, M.; Wu, Y.; Danyal, A.; Guo, B. Effect of unsaturated soil water transport function li nearization for mulched drip irrigation. *Soil Tillage Res.* **2024**, *237*, 105964. [CrossRef]
62. Du, B.; Qu, Z.; Yu, J.; Sun, G.; Shi, J. Experimental study on crop coefficient under mulched drip irrigation in Hetao Irrigation District of Inner Mongolia. *J. Irrig. Drain* **2014**, *33*, 16–20.
63. Shu-ming, B.; Zhong-yan, H.; Yu, W. Experimental Studies on the Orderliness of Water Requirement and Irrigating Effects of Maize in Yunnan. *Chin. J. Agrometeorol.* **2003**, *24*, 4.
64. Wendt, C.; Onken, A.; Wilke, O.; Hargrove, R.; Bausch, W.; Barnes, L. Effect of irrigation systems on the water requirements of sweet corn. *Soil Sci. Soc. Am. J.* **1977**, *41*, 785–788. [CrossRef]
65. Wang, J.; Cai, H.; Kang, Y.; Chen, F. Ratio of soil evaporation to the evapotranspiration for summer maize field. *Trans. CSAE* **2007**, *23*, 17–22.
66. Wang, H.; Tan, G.; Sun, Q.; Zhou, H. Variation of spring corn water requirement and its relaionship with the meteorological factors in Chengde, Hebei province. *J. Meteorol. Environ.* **2012**, *28*, 4.

67. Junfu, X.; Zhandong, L.; Yumin, C. Study on the water requirement and water requirement regulation of maize in China. *J. Maize Sci.* **2008**, *4*, 21–25.
68. Fan, X. *Study on Maize Water Requirement and Optimize Irrigation System under Different Water Stress*; Inner Mongolia Agricultural University: Inner Mongolia, China, 2013.